Polymer 51 (2010) 5788–5798

Contents lists available at ScienceDirect

Polymer

journal homepage: www.elsevier.com/locate/polymer

Brill transition and melt crystallization of nylon 56: An odd–even polyamide with two hydrogen-bonding directions

Laura Morales-Gámez, David Soto, Lourdes Franco, Jordi Puiggalí*

Departament d'Enginyeria Química, Universitat Politècnica de Catalunya, Av. Diagonal 647, E-08028 Barcelona, Spain

ARTICLE INFO

Article history:
Received 28 July 2010
Received in revised form
25 September 2010
Accepted 29 September 2010
Available online 8 October 2010

Keywords:
Polyamides
Brill transition
Crystallization

ABSTRACT

Brill transition and crystallization behaviour of nylon 56, a representative polymer of odd–even polyamides, were investigated by simultaneous WAXD and SAXS synchrotron radiation. Nylon 56 crystallized from solution into a peculiar structure where hydrogen bonds were established along the two directions. Nylon 56 experimented on heating a Brill transition that lead to a pseudohexagonal packing and lately to a monoclinic unit cell where neighbouring molecular segments were shifted along the chain axis direction. In disagreement with conventional polyamides, the Brill transition of nylon 56 was not reversible since on cooling the pseudohexagonal arrangement was mainly attained. Optical microscopy studies performed under both isothermal and non-isothermal conditions demonstrated that nylon 56 spherulites had different optical properties than even–even nylons having conventional sheet structures. The birefringence sign changed in the sequence positive–negative–positive when crystallization temperature was decreased.

1. Introduction

Aliphatic polyamides derived from odd diamines and even dicarboxylic acids (i.e. odd–even nylons) cannot establish all possible intermolecular hydrogen-bonding interactions when molecular chains have an all trans conformation (Fig. 1a). In this way, the conventional α/β forms usually found in commercial even–even nylons [1,2] (e.g. nylon 66) cannot be expected considering the minimization of the packing energy. These conventional structures are based on a stacking of sheets composed of hydrogen-bonded molecular chains with a planar zig-zag conformation. The corresponding fiber diffraction patterns are mainly characterized by two strong equatorial reflections at approximately 0.44 and 0.38 nm which are related to interchain distances within and between sheets, respectively.

A pseudohexagonal structure, which fiber diffraction pattern is characterized by a single strong equatorial reflection at approximately 0.415 nm, has been postulated for polyamides derived from an odd diamine and/or an odd dicarboxylic acid [1,3] (e.g. nylon 77). In this case, the torsional angles of the bonds adjacent to the amide groups tend to be $\pm 120°$, causing a tilt of the amide plane by approximately 60°, a shortening of the chain length and the establishment of good hydrogen-bonding interactions along a single direction.

However, it has recently been demonstrated that typical spacings of the α/β forms can surprisingly be found in nylons derived from odd diamines (e.g. nylons 56 [4], 92 [5] and 5–10 [6]) or odd dicarboxylic acids (e.g. nylons 65 [7] and 69 [8]). These structures were observed in both stretched fibers and single crystals obtained from diluted solutions. Structural studies on this kind of polyamides revealed a peculiar arrangement characterized by the establishment of intermolecular hydrogen bonds along two different directions. Basically, the molecular conformation was close to the all trans since only a slight deviation towards 150° (or −150°) for the two torsional angles vicinal to the odd diamide unit was necessary to face all NH and CO groups of neighbouring chains. The two amide groups of the odd unit rotated in opposite senses from the plane defined by the methylene carbon atoms allowing the establishment of good hydrogen-bonding interactions when neighbouring chains became conveniently shifted along the chain axis direction (Fig. 1b). In this way, a monoclinic unit cell containing two molecular segments was derived and the chain axis projection corresponded to a rectangular unit cell.

Conventional polyamides usually have a temperature induced transition towards a pseudohexagonal unit cell (γ' form). This transition can be easily detected in the X-ray diffraction patterns since the two strong equatorial reflections characteristic of the sheet structure gradually merge by increasing temperature into a single

* Corresponding author. Tel.: +34 93 4016684; fax: +34 93 4010978.
E-mail address: Jordi.Puiggali@upc.es (J. Puiggalí).

0032-3861/$ – see front matter © 2010 Elsevier Ltd. All rights reserved.
doi:10.1016/j.polymer.2010.09.074

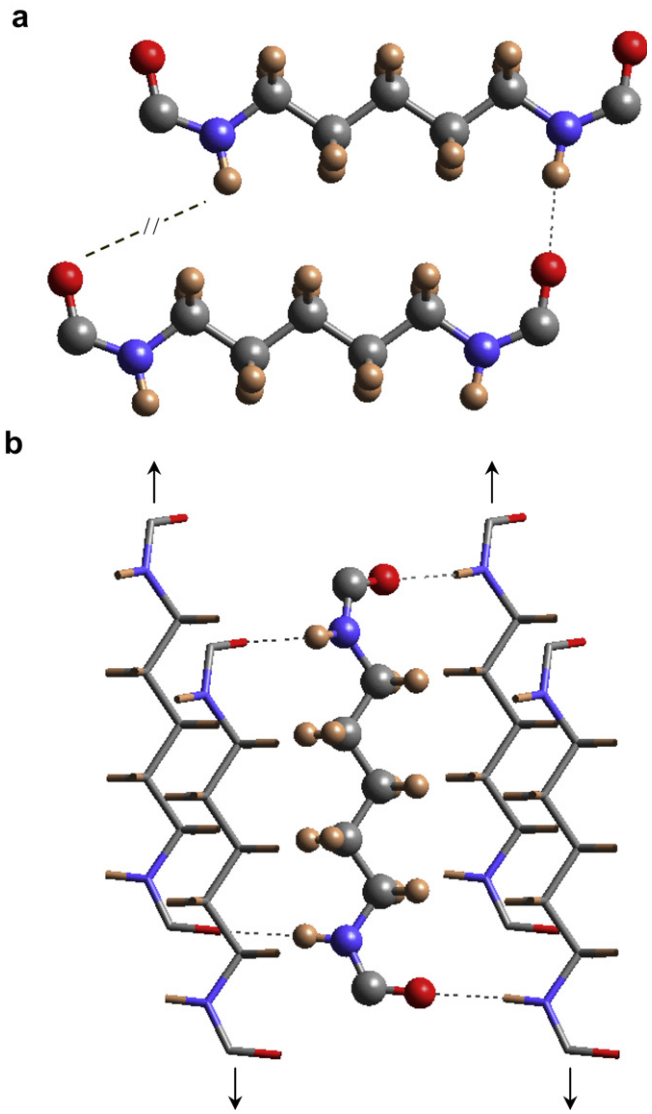

Fig. 1. (a) Scheme of the unfavorable hydrogen-bond geometry between odd diamide units of nylon 56 molecular chains with an all trans conformation. (b) Scheme of the establishment of hydrogen bonds along two directions when consecutive amide planes of a molecular chain slightly rotate in opposite directions from the plane defined by the methylene carbon atoms. External chains (stick representation) should be shifted along the chain axis direction (see arrows) with respect to the central chain (ball and stick representation), thus giving rise to a monoclinic unit cell. Color code: nitrogen, blue; oxygen, red; carbon, gray; hydrogen, brown. (For interpretation of the references to colour in this figure legend, the reader is referred to the web version of this article).

reflection. The Brill transition temperature just defines the moment in which this pseudohexagonal packing is reached. Brill temperature depends on the sample history and is also observed with a hysteresis effect when samples are cooled from the melt state. Although, a large number of studies on the Brill transition have been reported for several nylons [9–20], the phenomenon is not yet fully understood and different explanations have been postulated. Most of them suggest that hydrogen bonds are not disrupted during the Brill transition and explain the pseudohexagonal packing as a consequence of the increasing mobility of the polymethylene segments [21,22]. At this stage, it seems highly interesting to bring new data about the Brill transition and the crystallization process of the above indicated polyamides. Nylon 56 has been chosen as a representative odd–even polyamide with a peculiar hydrogen-bonding scheme. Nowadays, works concerning to odd–even polyamides are limited to nylons 11–10 and 11–12 which are derived from units with a large number of methylene units [23].

2. Experimental section

2.1. Materials

Nylon 56 was synthesized by interfacial polycondensation of 1,5-diaminopentane and adipoyl dichloride using toluene as organic solvent and sodium hydroxide as proton acceptor following the procedure previously described in Ref. [4]. An intrinsic viscosity of 0.7 dL/g was determined in dichloroacetic acid at 25 °C.

2.2. Measurements

Calorimetric data were obtained by differential scanning calorimetry using a TA Instruments Q100 series with T_{zero} technology and equipped with a refrigerated cooling system (RCS) operating at temperatures from −90 °C to 550 °C. Experiments were conducted under a flow of dry nitrogen with a sample weight of approximately 5 mg, while calibration was performed with indium. The T_{zero} calibration involved two experiments: the first was done without samples and the second was performed with sapphire disks.

The spherulite growth rate was determined by optical microscopy using a Zeiss Axioskop 40 Pol light polarizing microscope equipped with a Linkam temperature control system configured by a THMS 2600 heating and freezing stage connected to an LNP 94 liquid nitrogen cooling system. Spherulites were grown from homogeneous melt-crystallized thin films produced by melting 1 mg of the polymer mixture on microscope slides. Next, small sections of these films were pressed or smeared between two cover slides and inserted in the hot stage. The thicknesses of the squeezed samples were close to 10 μm in all cases. Samples were kept at 265 °C (more than 10 °C above the polymer melting point of 251–252 °C) for 5 min to wipe out sample history effects, and then quickly cooled to the selected crystallization temperature. Alternatively samples were no isothermally crystallized at different cooling rates (8, 1 and 0.5 °C/min) to increase the crystallization temperature range. The radius of the growing spherulites was monitored in both isothermal and non-isothermal crystallizations by taking micrographs with a Zeiss AxiosCam MRC5 digital camera at appropriate time intervals. A first-order red tint plate was employed to determine the sign of spherulite birefringence under crossed polarizers.

X-ray fiber diffraction data were obtained with Ni-filtered CuK_{α} radiation of wavelength 0.1542 nm from an Enraf Nonius rotating anode X-ray generator and using a modified Statton camera (W.H. Warhus, Wilmington, DE). Patterns were recorded at different temperatures using a temperature-controlled chamber provided by the manufacturer. Oriented fiber samples were obtained by drawing the polymer melt and performing a subsequent annealing under stress at 90 °C.

Simultaneous time-resolved SAXS/WAXD experiments were carried out at the CRG beamline (BM16) of the European Synchrotron Radiation Facility of Grenoble. The beam was monochromatized to a wavelength of 0.098 nm. The capillary with the sample was held in a Linkam hot stage with temperature control within 0.1 °C. WAXD/SAXS profiles were acquired during heating and non-isothermal crystallization experiments in time frames of 12 s. The heating and cooling rates varied between 20 and 8 °C/min, respectively. Two linear position-sensitive detectors were used [24]: The SAXS detector was calibrated with different orders of diffraction from silver behenate whereas the WAXD detector was calibrated with diffractions of a standard of an alumina (Al_2O_3) sample. The diffraction profiles were normalized to the beam

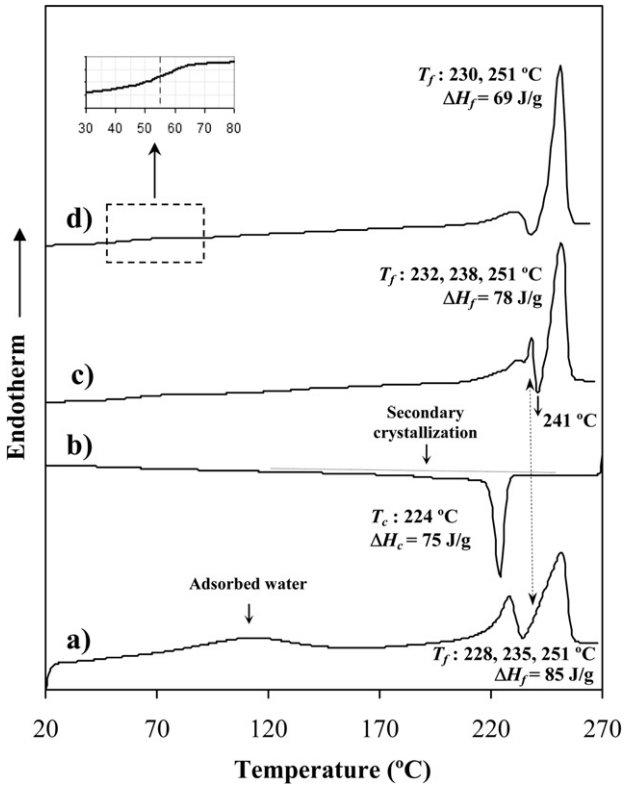

Fig. 2. Sequence of DSC curves corresponding to a heating run of a solution crystallized sample (a), cooling run from the melt state (b), heating run of a melt-crystallized sample (c) and heating run of a quenched sample (d). Heating runs were performed at 20 °C/min whereas the cooling run was performed at 10 °C/min. Inset shows a magnification of the glass transition.

intensity and corrected considering the empty sample background. Deconvolution of WAXD peaks was performed with the PeakFit v4 program by Jandel Scientific Software using a mathematical function known as "Gaussian area".

3. Results and discussion

3.1. Thermal properties of nylon 56

Fusion of a nylon 56 sample directly obtained from synthesis was characterized by two melting peaks that appeared in the 228–251 °C temperature range (Fig. 2a). It should be pointed out that the high temperature melting peak was very broad and asymmetric, suggesting that it was really derived from the overlapping of two signals (peaks 2 and 3). Thus, fusion of nylon 56 seemed to be characterized by a complex behaviour. The DSC heating trace showed also a very broad endothermic peak (80–140 °C) which could be assigned to adsorbed water since it was not detected in later heating runs, and furthermore a polymorphic transition could be discarded in this temperature range as then will be explained.

Nylon 56 crystallized easily during cooling runs from the melt state (e.g. an exothermic peak at 224 °C was detected at a cooling rate of 10 °C/min) giving rise to samples with a different melting behaviour. Thus, a posterior heating trace showed clearly as the broad high temperature peak was split in two peaks (peak 2 at 238 °C and peak 3 at 251 °C) and that an exothermic peak indicative of a recrystallization process appeared (241 °C). The low temperature melting peak (peak 1 at ca. 232 °C) could still be observed although with a very low intensity. Heating traces of melt quenched

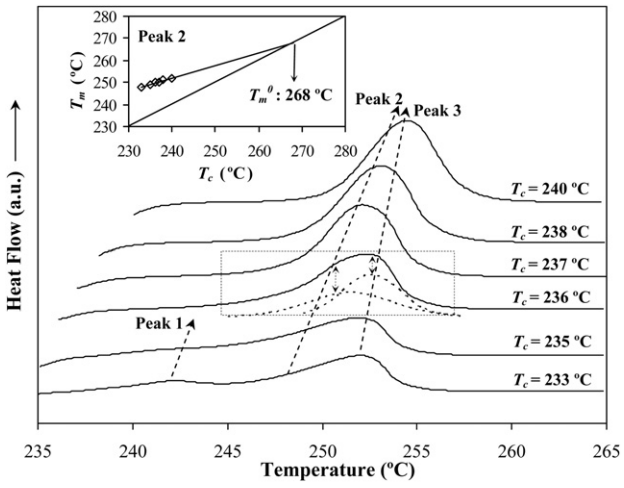

Fig. 3. Melting peaks for isothermally melt-crystallized samples. Deconvoluted profile is only shown for the sample crystallized at 236 °C (dashed box). The inset shows the Hoffman–Weeks plot drawn for the crystallization temperature dependent melting peak (peak 2).

samples clearly indicate that a completely amorphous sample could not be obtained at the maximum cooling rate allowed by the equipment. However, the glass transition temperature was detected at a temperature close to 55 °C. It is relevant that the melting behaviour was slightly different than observed for melt and solution crystallized samples since peak 2 was not detected. This feature suggests that peak 3 could be associated to thickest lamellae mainly produced during the heating process as a consequence of a melt/recrystallization of the thinner lamellae. This peak should be enhanced when more imperfect lamellae susceptible of reorganization were obtained as presumable in the melt quenched samples. The nature of peak 1 is more intriguing since at this stage two alternatives may be considered: a) the existence of very defective crystals and b) a polymorphic transition around 225–230 °C.

Fig. 3 shows the heating traces of samples previously isothermally crystallized from the melt state at different temperatures. Peaks 2 and 3 appear generally overlapped and consequently is difficult to differentiate the two melting processes. However, it can be stated that peak 2 increased on intensity and shifted to higher temperatures when crystallization temperature did, whereas peak 3 remained at a practically constant temperature. This feature is consistent with the indicated melt/reorganization process where thinner lamellae convert into thicker ones. Furthermore, it is possible to infer the equilibrium melting temperature of nylon 56 by considering the temperature evolution of peak 2 with crystallization temperature. In this way, the Hoffman–Weeks plot [25] displayed in the inset of Fig. 3 indicates an extrapolated equilibrium temperature of 268 °C, which is close to the value of 266 °C previously postulated [26] from theoretical considerations based on the spherulite grown model forwarded by Hoffmann–Weeks [25]. Heating runs show also the presence of the low temperature peak 1, but only when samples were isothermally crystallized at temperatures equal or lower than 235 °C. Thus, this value is a limit for a possible crystalline transition or for the development of the indicated defective crystals.

Isothermal experiments allowed the determination of the overall crystallization kinetics, which depends on primary nucleation and crystal growth, for a very restrictive temperature range due to the experimental limitations caused by the high speed of the crystallization process.

The time evolution of the relative degree of crystallinity, $\chi(t)$ was determined from hot crystallization exotherms (Fig. 4a)

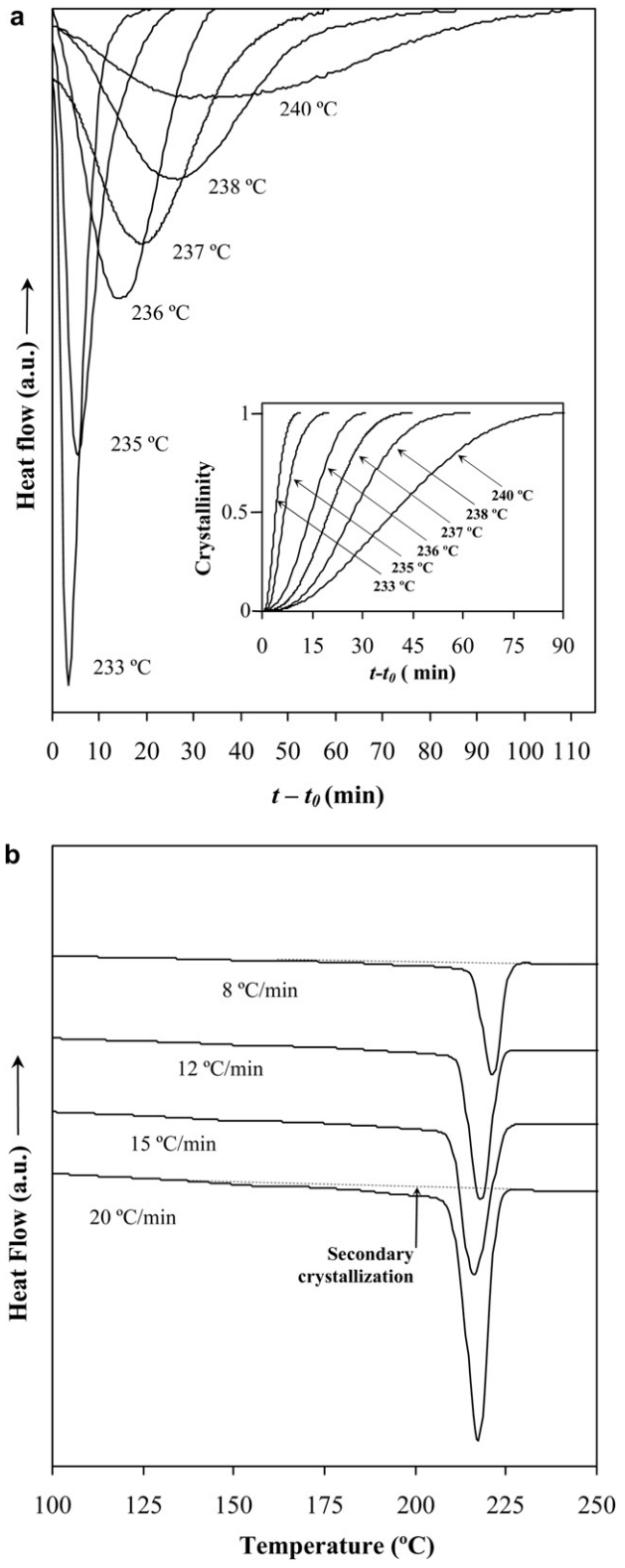

Fig. 4. (a) Exothermic DSC peaks corresponding to the hot isothermal crystallizations performed between 233 and 240 °C. Inset shows the development of relative crystallinity over time for isothermal crystallizations performed between 233 and 240 °C. (b) Dynamic DSC curves obtained at the indicated rates for the hot crystallization of nylon 56.

Table 1
Isothermal crystallization kinetic parameters deduced from DSC experiments for nylon 56.

T_c (°C)	n	$Z \times 10^8$ (s^{-n})	$k \times 10^3$ (s^{-1})	$1/\tau_{1/2}$ 10^3 (s^{-1})
233	2.34	217.1	3.80	4.17
235	2.57	17.8	2.36	2.33
236	2.80	0.396	0.998	1.17
237	2.64	0.511	0.723	0.83
238	2.52	0.601	0.547	0.55
240	2.15	3.79	0.353	0.42

through the ratio area of the exotherm up to time t divided by the total exotherm area, i.e.:

$$\chi(t) = \int_{t0}^{t} (dH/dt)dt / \int_{t0}^{\infty} (dH/dt)dt \quad (1)$$

where dH/dt is the heat flow rate and t_0 is the induction time. The development of crystallinity always showed a characteristic sigmoidal dependence on time, as plotted in the inset of Fig. 4a for six hot crystallization experiments.

Kinetic crystallization data were analyzed assuming the well known Avrami equation [27,28] for primary crystallization:

$$1 - \chi(t) = \exp\left[-Z \cdot (t - t_0)^n\right] \quad (2)$$

where Z is the temperature dependent rate constant and n is the Avrami exponent whose value varies according to the crystallization mechanism. A normalized rate constant, $k = Z^{1/n}$, is usually evaluated for comparison purposes since its dimension (time^{-1}) is independent of the value of the Avrami exponent.

Table 1 summarizes the main kinetic parameters of the primary crystallization process, which were deduced from the plots of log {-ln[1 − $\chi(t)$]} against log ($t - t_0$). The values of the Avrami exponent for the hot isothermal crystallizations lie in a narrow range, from 2.15 to 2.80, 2.50 being the average value. This suggests a predetermined (heterogeneous) nucleation with spherical growth that occurred under slight geometric constraints since the theoretical value should be equal to 3. Both sporadic (heterogeneous) and homogeneous nucleation can be clearly discarded as a higher exponent, close to 4, should be derived and furthermore these nucleation mechanisms should mainly be favoured at high undercoolings.

The values of the reciprocal of the crystallization half-time, $1/\tau_{1/2}$, are also summarized in Table 1. This parameter is a direct measure of the crystallization process, and could therefore be used to check the accuracy of the Avrami analyses. In this way, a similar dependence with the crystallization temperature was found for this parameter and the kinetic rate constant, demonstrating the suitability of the deduced Avrami values.

Fig. 4b shows the crystallization exotherms obtained during cooling runs performed at the different rates used in the synchrotron radiation experiments. A well defined peak is always observed within a narrow temperature range, which obviously shifts to lower temperatures by increasing the cooling rate. However, it is interesting to note that peaks had a long tail which could be associated to a secondary crystallization process and which was more clearly observed at high cooling rates.

3.2. Brill transition of nylon 56 on heating/cooling processes

Fiber diffraction patterns of nylon 56 were mainly characterized by strong equatorial reflections at 0.432 and 0.375 nm and an off meridional reflection at 1.272 nm (inset of Fig. 5), which were

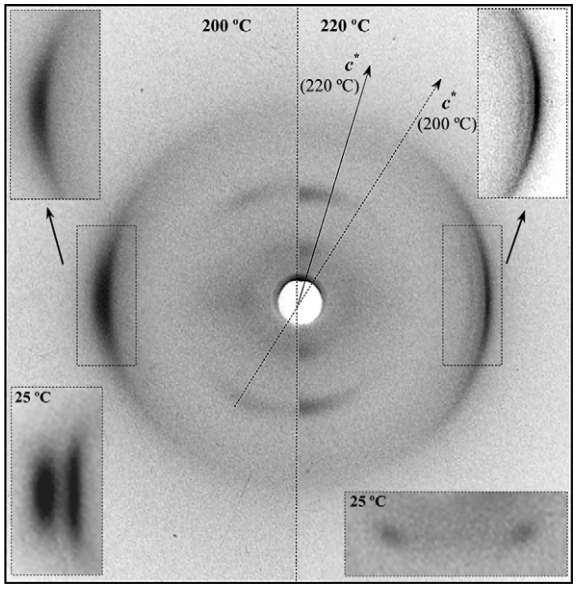

Fig. 5. X-ray fiber diffraction patterns of nylon 56 at 200 °C (left) and 220 °C (right). Insets show the equatorial reflections observed at 25, 200 and 220 °C and the 002 reflections (second layer line) observed at 25 °C.

indexed as the (020) and (110) reflections on the basis of a monoclinic unit cell with $a = 0.512$ nm, $b = 0.864$ nm, c (chain axis) = 3.133 nm and $\beta = 125.7°$ (form I) [4]. Structural modelling based on the diffraction data and energy calculations pointed towards the indicated model based on the establishment of two hydrogen-bonding directions [4].

Fig. 5 shows the X-ray fiber diffraction patterns of a nylon 56 sample taken under stress at 200 °C and 220 °C. At 200 °C the pattern shows only one strong and diffuse equatorial reflection at 0.423 nm, which is an indication that the Brill transition took place. It is interesting to note that 00*l* reflections still appeared with an off meridional orientation which is an indication that the structure obtained at 200 °C differed from a pseudohexagonal structure usually postulated for conventional polyamides. These 00*l* reflections seemed to have a close to meridional orientation in the patterns obtained at 220 °C, although it is difficult to determine the cc^* angle due to their arched appearance and the overlapping between 00*l* and 00$\bar{l}$ reflections. In this case, the new additional equatorial reflections observed at 0.454 nm and 0.436 nm are highly significant since they allow to discard again a pseudohexagonal structure. Previous works suggested that at high temperature a monoclinic structure (form II) with $a = 0.551$ nm, $b = 0.846$ nm, c (chain axis) = 3.133 nm and $\beta = 112.6°$ was achieved [4]. Note that the cc^* angle was 35.7° at room temperature whereas it decreased to 22.6° at 220 °C justifying the close meridional orientation detected for the 00*l* reflections.

Fig. 6 shows three-dimensional representations of WAXD profiles obtained by synchrotron radiation during a heating process performed at 12 °C/min from room temperature to fusion (q is the scattering vector given by $[4\pi / \lambda] \sin(\theta)$ or $2\pi / d_B$ where θ and d_B are the scattering angle and the Bragg spacing, respectively). Similar temperature dependent profiles were observed at heating rates of 8, 12, 15 and 20 °C/min. Profiles showed that the spacings of the two equatorial reflections at 0.433 and 0.374 nm gradually merged into a single peak at 0.423 nm that was reached at a temperature close to 200 °C. This process seems a typical Brill transition where a pseudohexagonal packing (γ^*-form) is favoured at a temperature slightly lower than the melting point. It is worth mentioning that the Brill transition temperature of nylon 56 was practically independent of the heating rate as shown in Fig. 7. After

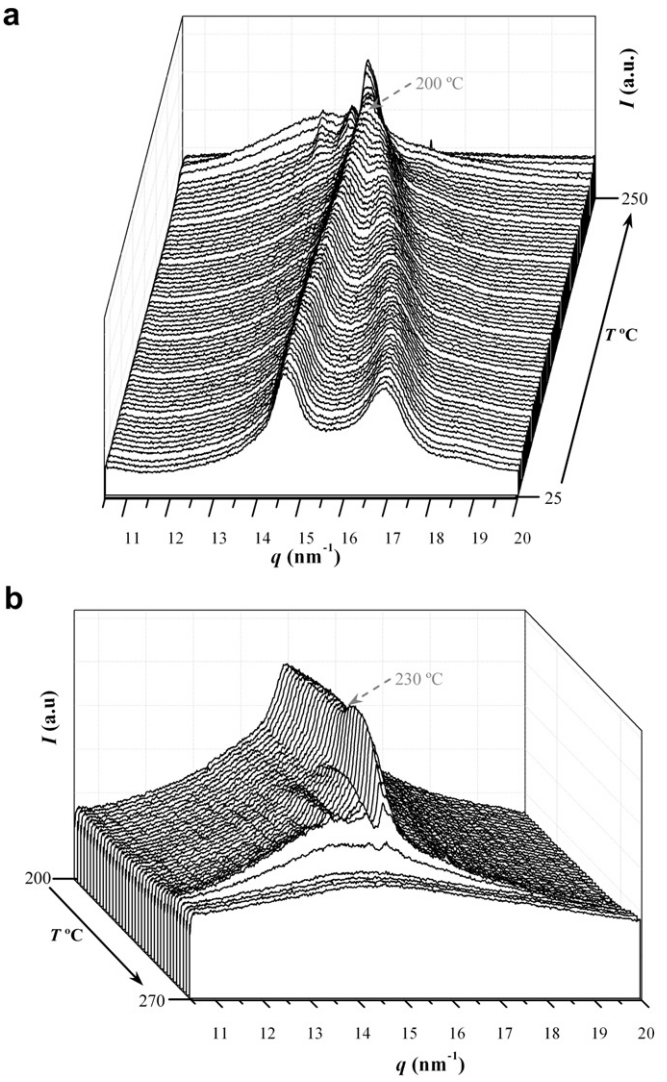

Fig. 6. Three-dimensional representations of WAXD profiles of nylon 56 during cooling (12 °C/min) from the melt to room temperature. All the temperature range is showed in (a), whereas a different view covering only the last frames (starting from 200 °C) is shown in (b).

the Brill transition, new peaks (e.g. those above indicated at 0.454 nm and 0.436 nm) started to appear as shown in Fig. 6b and a transition towards the indicated form II took place. All equatorial reflections became narrower (Fig. 5) and increased on intensity (Fig. 6b) during heating above the Brill transition temperature and before to start the melting process. Transition to form II occurred in a temperature range that was slightly lower (5 °C) than the endothermic peak 1 observed in the calorimetric analyses. In this way, this small melting peak seems to be related to highly defective crystals formed between bundles of lamellae, a conclusion that has been reported for different polyamides [29–31].

Fig. 8 compares the deconvoluted WAXD profiles representative of the structures attained at room temperature, at the Brill transition temperature and at a temperature close to fusion. In all cases, two amorphous halos (average values of 0.420 nm and 0.375 nm) were detected. However, the position of the maxima changed with temperature (i.e. the maximum of the first halo appeared at 0.409 and 0.430 nm in the patterns taken at 25 and 230 °C, respectively). This feature suggests that the amorphous phase has a more compact molecular arrangement when temperature decreases, as it will be discussed in the next section. In fact, a similar increase in the

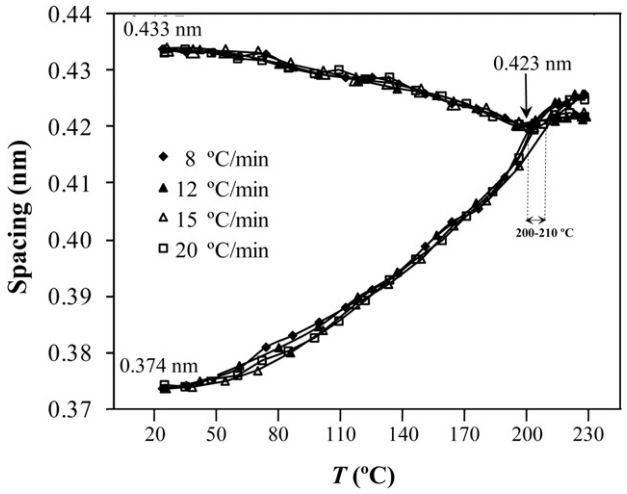

Fig. 7. Plot showing the temperature evolution of the spacings corresponding to the two strongest equatorial reflections at different heating rates.

average interchain distance in the amorphous phase above the Brill transition temperature was reported and analyzed in detail for nylon 66 [17].

It is worth pointing out that Bragg reflections were very broad while temperature was lower or equal than the Brill transition temperature. Assuming that the low temperature structure (form I) is defined by a molecular arrangement where hydrogen bonds are established along two directions, it seems reasonable to expect clear differences on heating between conventional polyamides and nylon 56. Thus, the pseudohexagonal structure [20,32,33] (γ' form) attained with nylons characterized by a single hydrogen-bond direction could not be observed in the diffraction patterns of nylon 56. Transitions induced by temperature on this polyamide may involve only slight changes in the torsional angles vicinal to amide groups or even an increase in the mobility of polymethylene segments without disrupting the initial hydrogen-bonding scheme. Note that the chain axis projection may correspond to a pseudohexagonal packing, as deduced from the single equatorial reflection at the Brill transition temperature, but a chain axis shift still remained between neighbouring chains. In this sense, fiber patterns with non-meridional 00*l* reflections are essential to support the finding that the Brill structure is different from the conventional γ′ form.

Fig. 9a shows the WAXD profiles acquired during a cooling run (10 °C/min) from the melt state. It is clear that nylon 56 crystallized into the form II characterized as above indicated by multiple narrow reflections with an equatorial or close equatorial orientation. Note that the profile showed in Fig. 9b is practically identical to that attained during the heating process (Fig. 8c) just at some degrees before fusion. Fig. 9a shows also that the reflection at ca. 0.423 nm does not split when temperature is lowered down to room temperature and consequently it could be deduced that the Brill transition is not reversible on cooling. WAXD profiles showed also that characteristic reflections of form II moves to lower spacings by decreasing the temperature and overlapped the main equatorial reflection at ca. 120 °C. Thus, the intensity of the reflection at 0.423 nm increased during cooling as well as the peak became broader.

It should be pointed out that the characteristic reflections of form I appeared in the first stage of crystallization and increased in intensity during the cooling process. Logically these peaks slightly moved to lower spacings due the contraction of the unit cell when temperature decreased. At room temperature the deconvoluted profile (Fig. 9c) was characterized by reflections associated to form I (0.440 and 0.383 nm) and reflections indicative of the pseudohexagonal packing (e.g. 0.419 nm) attained after the Brill transition

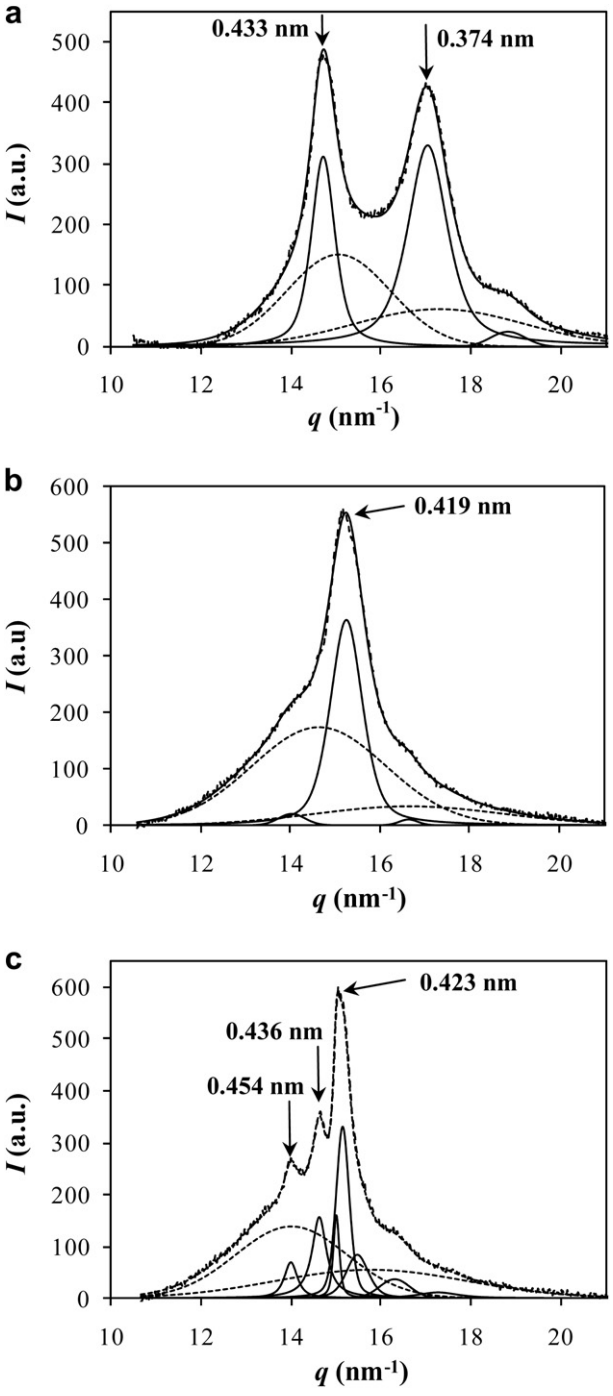

Fig. 8. One-dimensional WAXD profiles for nylon 56 taken at room temperature (a), 200 °C (b), and 230 °C (c) during a heating scan (12 °C/min). Spacings of main reflections are indicated together with the deconvoluted peaks.

temperature, which appeared predominant according to their relative intensity. It should also be indicated that form I could be completely recovered when fibers were annealed under stress at 90 °C or the samples were recrystallized from diluted formic acid/ethanol (1:4 *v*/*v*) solutions [4].

3.3. Non-isothermal crystallization studies by simultaneous SAXS/WAXD synchrotron radiation experiments

The crystallization process was simultaneously monitored by time-resolved WAXD and SAXS non-isothermal experiments. In

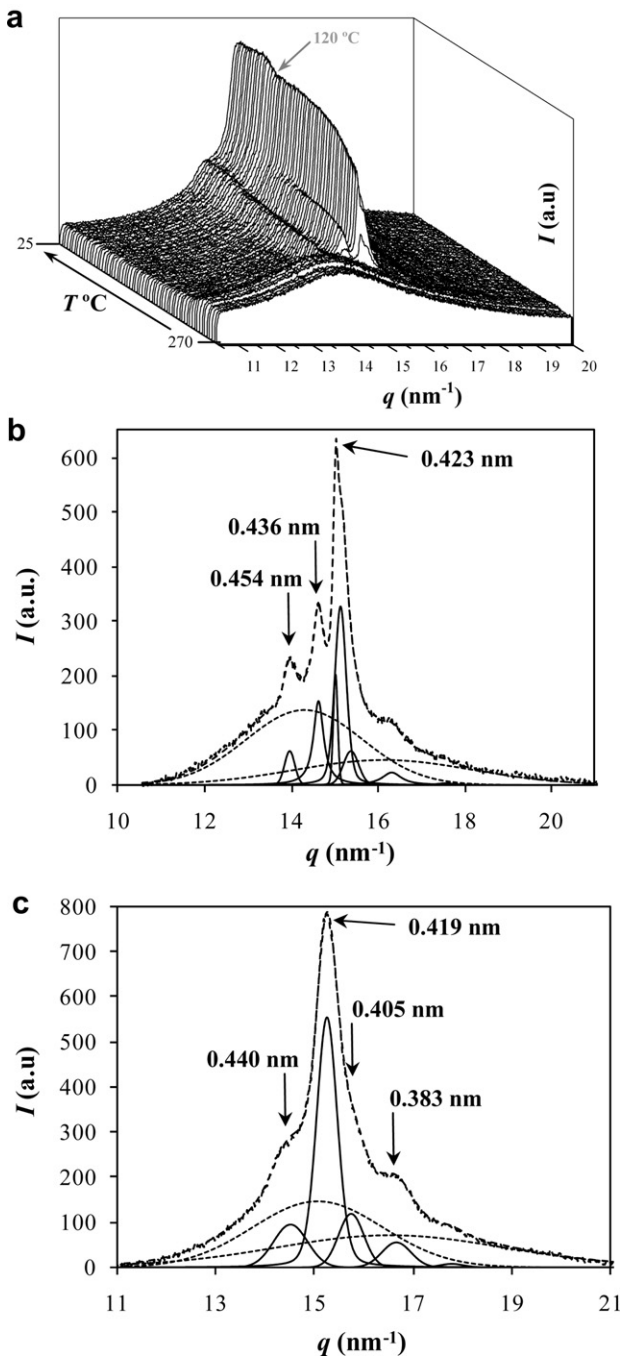

Fig. 9. (a) Three-dimensional representation of WAXD profiles of nylon 56 during cooling (12 °C/min) from the melt to room temperature. (b) and (c) One-dimensional WAXD profiles for nylon 56 taken at 220 °C (b) and at room temperature (c) during a cooling run (12 °C/min) from the melt state. Spacings of main reflections are indicated together with the deconvoluted peaks.

this way, the evolution of the mass fraction of the crystalline phase in the sample, X_C^{WAXD}, was determined from the different WAXD deconvoluted profiles as the ratio between the total intensities of the crystalline reflections I_c and the overall intensity I_T. Values at the end of crystallization ranged between 0.26 and 0.40 and increased with decreasing the cooling rate (Fig. 10).

Primary crystallization was very fast at all the assayed cooling runs and was completed within a range lower than 2 min after primary nuclei were formed (i.e. after achieving the induction time). Secondary crystallization was clearly dependent on the

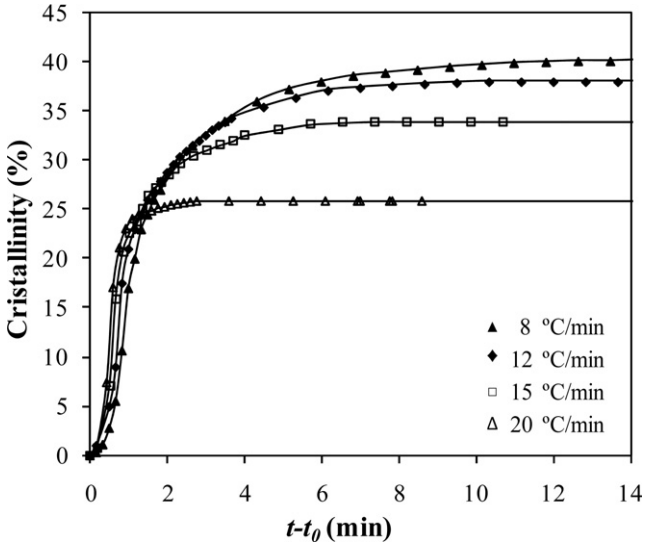

Fig. 10. Time evolution of WAXD crystallinity during non-isothermal hot crystallizations performed at the indicated cooling rates.

cooling rate and varied from 12 to 2 min for rates of 8 and 20 °C/min, respectively.

SAXS patterns showed a long period peak at a value of the scattering vector, q, close to 0.5–0.8 nm^{-1} after subtraction of the empty sample background observed near the beam stop (Fig. 11a). This peak, which can be attributed to the lamellar structure of the spherulites, started to appear at the same temperature than crystalline reflections in the WAXD patterns, as presumable for a crystallization process controlled by nucleation and crystal growth. This temperature obviously decreased with increasing the cooling rate.

SAXS data were analyzed by the normalized one-dimensional correlation function [34], $\gamma(r)$, which corresponds to the Fourier transform of the Lorentz-corrected SAXS profile:

$$\gamma(r) = \int_0^\infty q^2 I(q)\cos(qr)dq \Big/ \int_0^\infty q^2 I(q)dq \qquad (3)$$

The scattering intensity was extrapolated to both low and high q values using Vonk's model [35] and Porod's law, respectively.

Correlation functions (Fig. 11b) were used to determine the scattering invariant, Q, which allows evaluating the peak intensity evolution during crystallization, and morphological parameters like the long period, L_γ, crystalline lamellar thickness, l_c, and amorphous layer thickness, l_a.

The intensity of the SAXS peak increased during primary crystallization and then decreased. This observation is important because it suggests a change in the amorphous phase since the intensity of SAXS peaks depends on the degree of crystallinity but also on the difference between the electronic densities of amorphous and crystalline phases. It is clear that on cooling the amorphous interlamellar component should adopt a more compact molecular arrangement, probably as a result of the improved hydrogen-bonding interactions. Thus, the SAXS peak reached a maximum value before the start of secondary crystallization, as it will then be explained, and practically disappeared when crystallization was complete.

Fig. 12a shows the time evolution of the invariant, Q, for the different crystallization rates. The time corresponding to the maximum value for the invariant clearly diminished by increasing the cooling rate as well as the range where the secondary crystallization process took place.

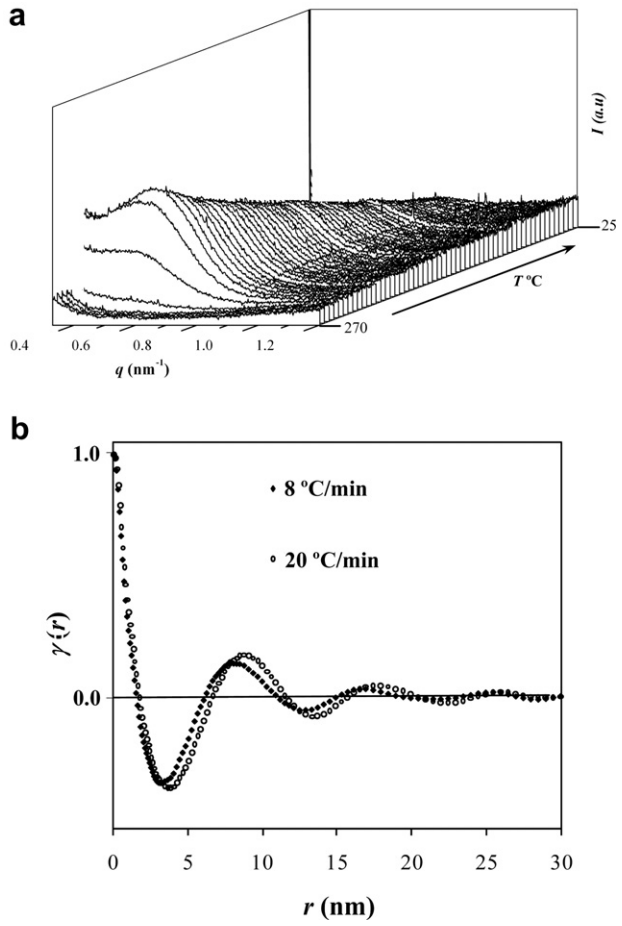

Fig. 11. (a) Three-dimensional representation of SAXS profiles of nylon 56 during cooling (12 °C/min) from 270 °C (melt state) to room temperature. (b) Correlation functions corresponding to the end of secondary crystallization obtained during cooling runs performed at the indicated rates.

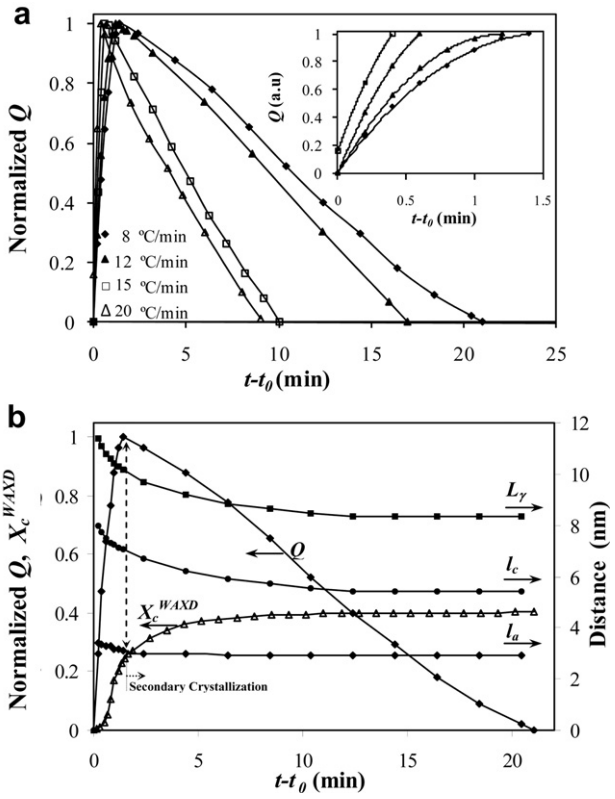

Fig. 12. (a) Temperature evolution of the scattering invariant, Q, at the indicated cooling rates. Inset shows its evolution during primary crystallization. (b) Temperature evolution of the long period, L_γ, crystal thickness, l_c, amorphous thickness, l_a, scattering invariant, Q, and degree of crystallinity, X^{WAXD}, during a non-isothermal melt crystallization performed at a cooling rate of 8 °C/min.

The evolution of morphological parameters during crystallization (Fig. 12b) shows a slight change in the long period (e.g. from 11.7 to 8.2 nm in the cooling performed at 8 °C/min), which is mainly due to the decrease in crystalline lamellar thickness (e.g. from 8.0 to 5.8 nm). The latter was also significant during the secondary crystallization step and indicates that new secondary lamellae inserted into the loosely stacked bundles of primary lamellae. New lamellae suffer spatial restrictions, leading to thinner defective crystals. Changes on the amorphous layer thickness mainly occurred during primary crystallization and were consistent with a reordering effect that conduced to a slight decrease (i.e. from 3.7 to 2.4 nm). It is worth pointing out that this thickness remained practically constant during the entire long time interval where secondary crystallization took place. Fig. 12b compares also the evolution of the invariant, Q, and the WAXD crystallinity allowing correlating the maximum value of the invariant with the end of the primary crystallization process.

Fig. 11b shows the correlation functions calculated for the SAXS profiles obtained at the minimum (8 °C/min) and the maximum (20 °C/min) assayed cooling rates and at the temperature (time) corresponding to the end of crystallization (i.e. the last frame which peak still allowed the calculation of the correlation function). Differences in lamellar spacings are a consequence of the balance between two counter factors: enhanced insertion mechanism producing thinner secondary lamellae, and increased crystallization temperature resulting in thicker primary lamellae by decreasing the cooling rate.

Fig. 13a compares the evolution of morphological parameters during crystallization for the different studied cooling rates, whereas cooling rate dependence of initial and final values of these parameters are shown in Fig. 13b. The increase observed for the lamellar spacing with the cooling rate indicates the prevalence of the lamellar insertion effect.

Fig. 11 also shows that the L_γ value associated with the most probable distance between the centers of gravity of two adjacent crystals (abscise of the first maximum of the correlation function) is greater than the long period determined from twice the abscise value of the first minimum of the correlation function, which is interpreted as the most probable distance between the centers of gravity of a crystal and its adjacent amorphous layer. This indicates a broader distribution of the layer widths of the major component [36], which corresponds to the crystal phase.

SAXS crystallinities, X^{SAXS}, in the 66–70% range were calculated at the end of secondary crystallization from the values of the morphological parameters ($l_c/(l_c + l_a)$). It is well known that the correlation function method cannot distinguish between l_c and l_a thicknesses, which certainly constitutes an uncertainty of this analysis. However, it is also clear that the linear degree of crystallinity (X^{SAXS}) must be always greater than the crystallinity determined from WAXD experiments (26–40%) since amorphous-rich interstack regions must exist [37,38]. Note, for example, that the crystallization performed at 8 °C/min had a X^{SAXS}/X_c^{WAXD} ratio lower than unity with the other assignment, which is not physically meaningful. High discrepancies between SAXS and WAXD crystallinities are usual in the literature [36] and have been explained

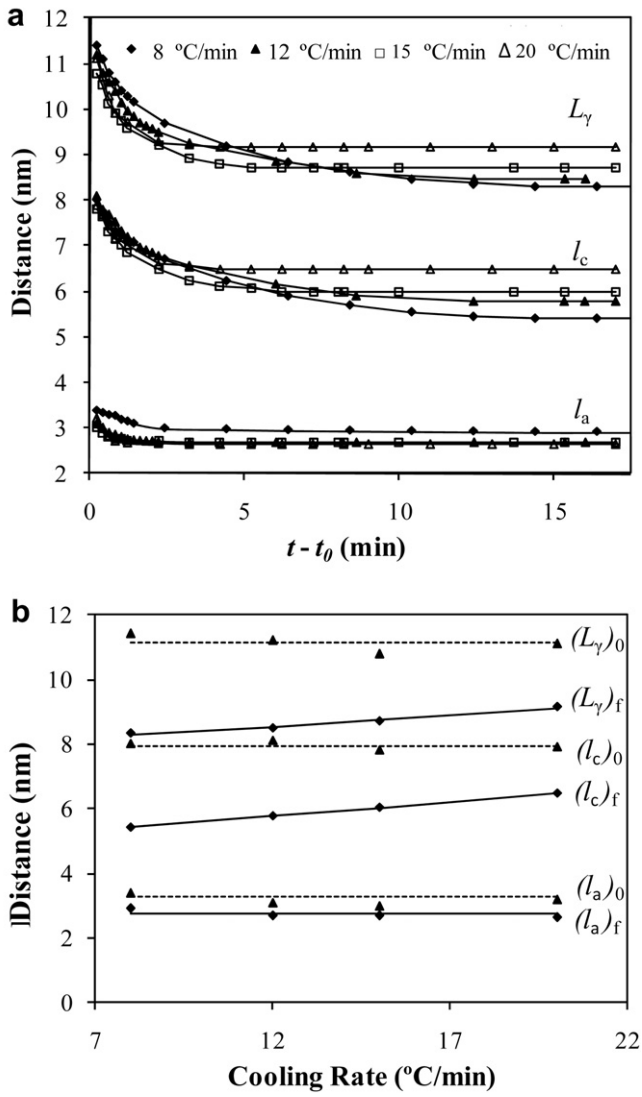

Fig. 13. (a) Evolution of L_γ, l_c and l_a values during non-isothermal crystallization at different cooling rates. (b) L_γ, l_c and l_a values obtained at the end (subscript f) and the beginning (subscript 0) of non-isothermal hot crystallization performed at different cooling rates.

assuming the existence of amorphous phase domains. Note also that the given assignment lead to a crystalline lamellar thickness, l_c, close to 6 nm which is higher than the chain axis repeat 3.133 nm and close to predicted values for similar polyamides [39]. Moreover, a lamellar thickness of only 2 nm is difficult to combine with the *hkl* reflections detected in the X-ray diffraction patterns.

3.4. Isothermal and non-isothermal crystallization studies by optical microscopy

Isothermal crystallization of nylon 56 from the melt rendered spherulites of appreciable size over the narrow temperature range of 238–220 °C (Fig. 14). This crystallization proceeded according to a heterogeneous nucleation as demonstrated by DSC analysis. The nucleation density increased exponentially with decreasing temperature in such a way that morphologies were difficult to examine at temperatures lower than 220 °C. Specifically, densities of 15, 40, 90, 160 and 210 nuclei/mm^2 were measured at crystallization temperatures of 239, 237, 234, 230 and 227 °C, respectively.

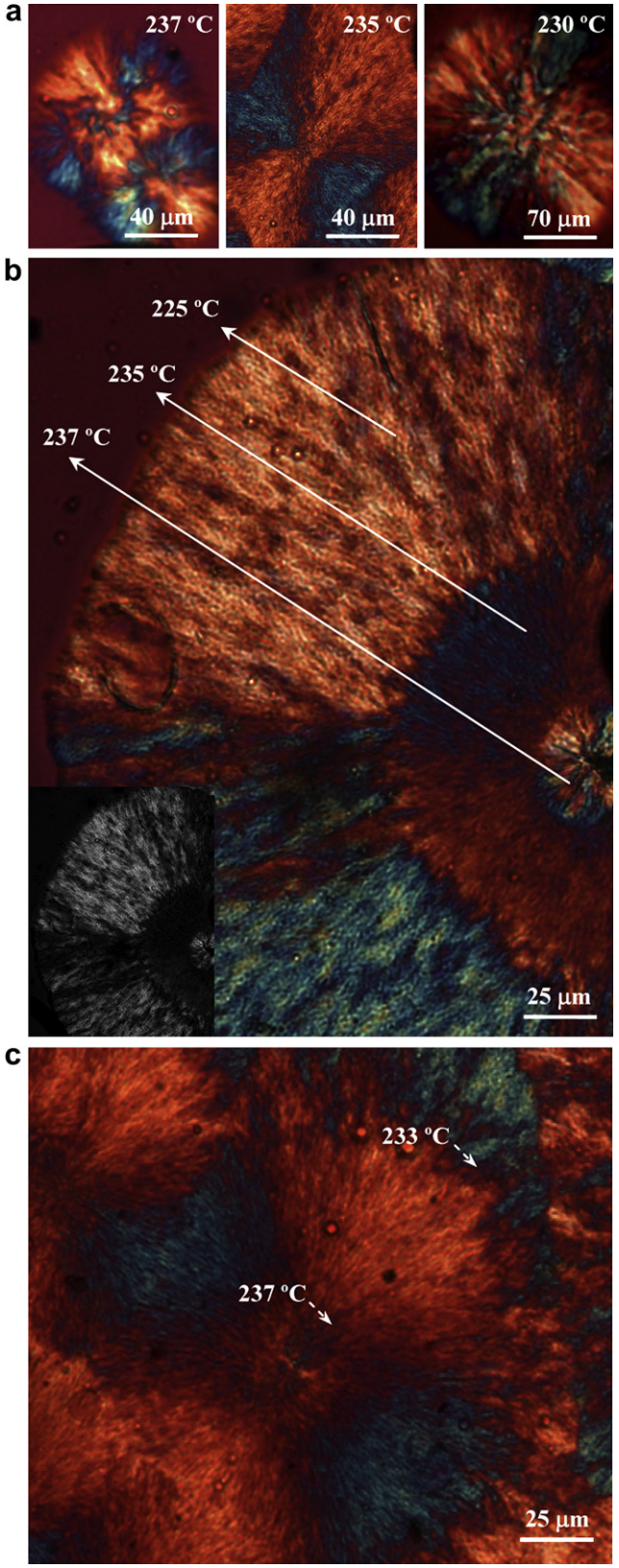

Fig. 14. (a) Optical micrographs of nylon 56 spherulites isothermally crystallized at 237 °C (left), 235 °C (middle) and 230 °C (right). (b) Optical micrograph of a nylon 56 spherulite that was isothermally crystallized at three different temperatures: Firstly at 237 °C, secondly at 235 °C and finally at 225 °C. Inset shows a black and white micrograph where the low birefringence zone corresponding to the polymer crystallized at the intermediate temperature appeared as a black ring. (c) Optical micrograph of a nylon 56 spherulite non-isothermally crystallized at a cooling rate of 1 °C/min.

Spherulites exhibited variable optical properties and a fibrillar texture over the studied temperature range (Fig. 14a). At temperatures higher than 237 °C spherulites showed a high positive birefringence, although aggregates with a non defined optical sign were also observed when temperature was higher than 237 °C. Negative spherulites with a low birefringence were developed in the narrow interval between 233 °C and 237 °C, whereas high positively birefringent spherulites were formed at temperatures lower than 233 °C. Spherulites isothermally growth in three steps at the corresponding representative temperatures (Fig. 14b) allowed to compare better the indicated optical properties and showed clearly that the birefringence sign changed in the sequence of positive–negative–positive when crystallization temperature was decreased. Furthermore, it can be observed (inset of Fig. 14b) that the low birefringence zone can also be detected as a black ring justifying previous observations were only positive spherulites were reported together with a zero birefringent zone at temperatures close to 233 °C [26]. Non-isothermal experiments (Fig. 14c) showed also the development of the three different birefringent zones with changes that took place at well defined temperatures (237 and 233 °C).

It is interesting to note that the indicated birefringence changes are different to those observed in conventional polyamides like nylon 66 where birefringence changed from negative to positive by decreasing the crystallization temperature. In this case, the change in the optical properties was explained considering the structure based on the stacking of hydrogen-bonded sheets and different growth geometries [40,41]. Thus, positive and negative spherulites were interpreted as a consequence of the establishment of hydrogen bonds along a radial or a tangential spherulitic direction, respectively. The birefringence sign was directly associated with how lamellae with a single structure grow in the spherulite. However, the reason for such a drastic change in the growth mechanism at a well defined temperature remains unclear. The peculiar structure found for the high temperature form of the studied odd–even nylon where two hydrogen-bonding directions seem to exist may be one of the reasons for the unusual formation of positive spherulites at higher crystallization temperature. In any way, the synchrotron data acquired during cooling runs allowed discarding a direct relation between the change on the birefringence sign and possible polymorphic transitions. Furthermore, no changes on both texture and birefringence could be detected when the different spherulites were heated until fusion. Thus, the morphologies developed during crystallization of nylon 56 were not reversible.

Spherulitic growth rates were determined from isothermal experiments by following the change of the spherulite radius with time up to impingement (Fig. 15) within the studied temperature intervals. The measured radial growth rates, G, varied from a minimum value of 0.08 μm/s at 239 °C to a maximum value close to 1.3 μm/s at 225 °C. Non-isothermal procedures were also applied to study the temperature dependence of the spherulitic growth rate during hot crystallization. Thus, the spherulitic growth rate (G) can be estimated [42–44] by measuring the change of the spherulite radius (R) with temperature (T) when experiments are performed at a constant cooling rate (dT/dt):

$$G = dR/dt/ = (dR/dT)\cdot(dT/dt) \quad (4)$$

Experimental problems lie in the choice of the cooling rate required to maximize the crystallization temperature range where radii can be well measured. For this reason, the use of various rates is highly effective in expanding this range.

The plot of the radius versus temperature (Fig. 15b) can be fitted to polynomial equations with a good regression coefficient (r) that

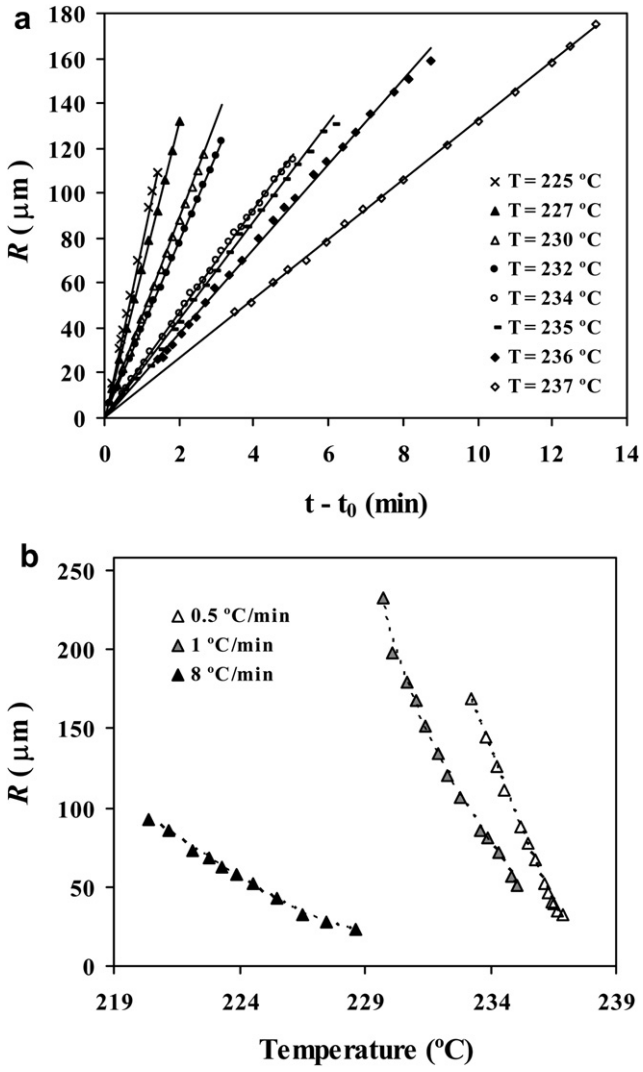

Fig. 15. (a) Plots of the radius of nylon 56 spherulites versus crystallization time for isothermal hot crystallizations performed at temperatures ranging between 225 and 237 °C. (b) Variation in spherulite radius with temperature during cooling at the indicated rates.

allows the calculation of the value of its first derivative (dR/dT) for each cooling rate as a function of the crystallization temperature. Third-order equations were always chosen since the regression coefficients (≥ 0.998) were slightly better than those calculated for lower-order equations and remained practically constant when higher orders were assayed.

Fig. 16b plots the deduced G values from non-isothermal data and those measured from isothermal experiments. It should be pointed out that a good agreement was found and that non-isothermal experiments had several advantages: a continuous evolution could be determined and measures were less time consuming.

Experimental data defined the right side of the typical bell shaped curve that describes the temperature dependence of the growth rate, i.e. the zone controlled by secondary nucleation. Both isothermal and non-isothermal measures suggest the existence of a shoulder at high temperatures (>233 °C), which may be a consequence of a different secondary nucleation constant. Thus, at least experiments pointed out to the existence of two crystallization regimes which could be associated to different spherulites, e.g. positive at temperatures lower than 233 °C and negative at higher temperatures.

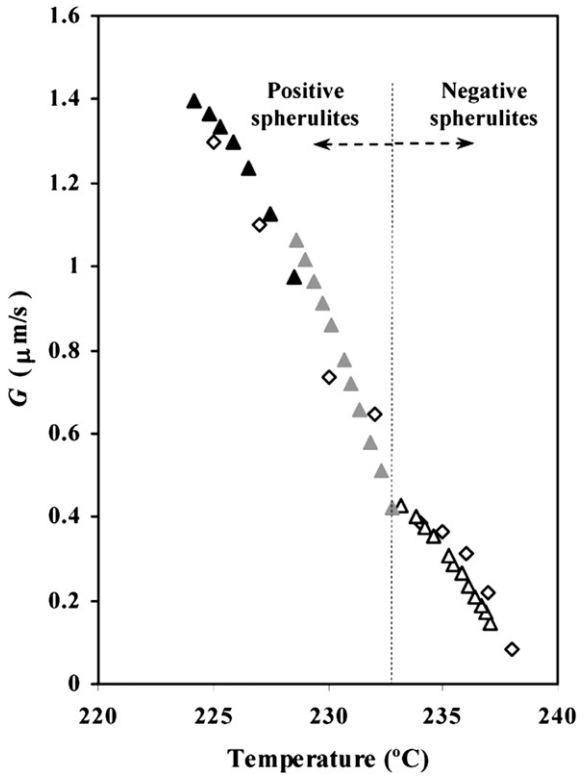

Fig. 16. Spherulitic growth rates determined by the equations deduced for cooling runs of 8 (▲), 1 (▲) and 0.5 °C/min (△). For the sake of completeness, experimental data deduced from isothermal experiments are also plotted (◇).

4. Conclusions

Nylon 56 crystallized from solution according to a peculiar monoclinic structure (form I) where hydrogen bonds were established along two directions and where neighbouring chains were shifted along their chain axis direction. On heating, this structure showed a Brill transition resulting in a pseudohexagonal chain axis projected unit cell and a structure where the chain axis shift was kept in order to optimize the hydrogen-bonding interactions. At some degrees before fusion, the diffraction patterns showed new narrow reflections which could be indexed according to a new monoclinic unit cell (form II).

Brill transition was not reversible since nylon 56 mainly crystallized from the melt into form II, which on cooling gave rise to a pseudohexagonal packing. A minor crystallization into form I could also be detected and accounted into a significant ratio of this form when room temperature was achieved.

Nylon 56 crystallized on cooling into fibrillar spherulites with optical properties that were depended on the crystallization temperature and differed from those found in nylons having conventional sheet structures. During crystallization thinner lamellae inserted into the loosely stacked bundles of primary lamellae and the interlamellar amorphous regions became more compact.

Acknowledgements

This research has been supported by a CICYT/FEDER and AGAUR grants (MAT2009-11503 and 2009SGR-1208). We want to express our gratitude to Drs. François Fauth and Ana Labrador of the CRG BM16 beamline staff of CELLS (Consortium for the Exploitation of the Synchrotron Light Laboratory). L. M. acknowledges finantial support from the Agència de Gestió d'Ajuts Universitaris i de Recerca.

References

[1] Bunn CW, Garner EV. Proc R Soc London Ser A 1947;189:39–68.
[2] Xenopoulos A, Clark ES. In: Kohan MI, editor. Nylonplastics handbook, Chap 5. Munich, Vienna and New York: Hanser Publishers; 1995. p. 108–37.
[3] Kinoshita Y. Makromol. Chem 1959;33:1–20.
[4] Puiggalí J, Franco L, Alemán C, Subirana JA. Macromolecules 1998;31:8540–8.
[5] Franco L, Subirana JA, Puiggalí J. Macromolecules 1998;31:3912–24.
[6] Villaseñor P, Franco L, Subirana JA, Puiggali J. J Polym Sci Part B Polym Phys Ed 1999;37:2383–95.
[7] Navarro E, Franco L, Subirana JA, Puiggalí J. Macromolecules 1995; 28:8742–50.
[8] Franco L, Cooper SJ, Atkins ADT, Hill M, Jones NA. Macromolecules 1998;36:1153–65.
[9] Holmes DE, Bunn CW, Smith D. J Polym Sci Part A, Gen Papers 1955;17: 159–77.
[10] Brill R. Makromol Chem 1956;18:294–309.
[11] Schmidt GF, Stuart HA. Naturforsch Z 1958;13A:222–6.
[12] Hirschinger J, Miura H, Gardner KH, English AD. Macromolecules 1990;23: 2153–9.
[13] Wendoloski JJ, Gardner KH, Hirschinger J, Miura H, English AD. Science 1990;247:431–6.
[14] Ramesh C, Keller A, Eltink SJEA. Polymer 1994;35:2483–7.
[15] Hill MJ, Atkins EDT. Macromolecules 1995;28(2):604–9.
[16] Vasanthan N, Murthy NS, Bray RG. Macromolecules 1998;31:8433–5.
[17] Murthy NS, Wang Z, Hsiao BS. Macromolecules 1999;32:5594–9.
[18] Ramesh C, Gowd EB. Macromolecules 1999;32:3721–6.
[19] Jones NA, Atkins EDT, Hill MJ. J Polym Sci Part B Polym Phys 2000;38:1209–21.
[20] Feldman AY, Wachtel E, Vaughan GBM, Weinberg A, Marom G. Macromolecules 2006;39:4455–9.
[21] Tashiro K, Yoshioka Y. Polymer 2004;45:6349–55.
[22] Yoshioka Y, Tashiro K, Ramesh C. Polymer 2003;44:6407–17.
[23] Cui X, Yan D. Eur Polym J 2005;41:863–70.
[24] Rueda DR, García-Gutiérrez MC, Nogales A, Capitán MJ, Ezquerra TA, Labrador A, et al. Rev Sci Instrum 2006;77. Art. No. 033904 Part 1.
[25] Hoffman JD, Weeks JJ. J Chem Phys 1962;37:1723–46.
[26] Magill JH. J Polym Sci Part A 1965;3:1195–219.
[27] Avrami M. J Chem Phys 1939;7:1103–12.
[28] Avrami M. J Chem Phys 1940;8:212–24.
[29] Wunderlich B. Macromolecular physics. In: Crystal melting, vol. 3. New York: Academic Press; 1980.
[30] Liu M, Zhao Q, Wang Y, Zhang C, Mo Z, Cao S. Polymer 2003;44:2537–45.
[31] Cui X, Qing S, Yan D. Eur Polym J 2005;41:3060–8.
[32] Biangardi JJ. Macromol Sci 1990;29:139–53.
[33] Jones NA, Atkins EDT, Hill M, Cooper SJ, Franco L. Polymer 1997;38:2689–99.
[34] Vonk CG, Kortleve G. Kolloid Z Z Polym 1967;220:19–24.
[35] Vonk CG. J Appl Cryst 1975;8:340–1.
[36] Hsiao BS, Wang Z, Yeh F, Yan G, Sheth KC. Polymer 1999;40:3515–23.
[37] Hsiao BS, Gardner KH, Wu DQ, Chu B. Polymer 1993;34:3986–95.
[38] Ikada Y, Jamshida K, Tsuji H, Hyoan SH. Macromolecules 1987;20:904–6.
[39] Dreyfuss P. J Polym Sci Part B Phys Ed 1973;11:201–16.
[40] Lovinger AJ. J Appl Phys 1978;49:5003–13.
[41] Lovinger AJ. J Appl Phys 1978;49:5014–28.
[42] Chen M, Chung CT. J Polym Sci Part B Polym Phys 1998;36:2393–9.
[43] di Lorenzo ML, Cimmino S, Silvestre C. Macromolecules 2000;33:3828–32.
[44] di Lorenzo ML. Polymer 2001;42:9441–6.